Modal Properties and Control System Design for Two-Link Flexible Manipulators

Christopher J. Damaren

The International Journal of Robotics Research 1998 17: 667
DOI: 10.1177/027836499801700606

Christopher J. Damaren
Department of Mechanical Engineering
University of Canterbury
Christchurch, New Zealand

Modal Properties and Control System Design for Two-Link Flexible Manipulators

Abstract

The vibration modes of a generic two-link flexible manipulator are studied as a function of the link, rotor, and tip (stator/payload) mass distribution. Necessary and sufficient conditions are developed for all vibration modes to exhibit a node at the manipulator endpoint. A rigorous treatment of the relevant kinematics and dynamics shows that this property can be closely achieved for large tip/link mass ratio and sufficiently small rotor inertia. The major impacts of this result on feedforward/feedback controller design are uncovered. First, the nonlinear joint torque to end-effector motion dynamics become essentially equivalent to those of the rigid case. Second, an output involving the endpoint rates and elastic motions is shown to possess the passivity property for suitably defined inputs. This permits the design of simple controllers that furnish endpoint stabilization with simultaneous vibration suppression. A numerical example is used to illustrate the results and demonstrate the achievable performance using the controller design concepts.

1. Introduction

The impact of structural flexibility on the analysis and control of lightweight robots presents a serious challenge to robotic engineers. However, this marriage of structural dynamics, nonlinear multibody dynamics, and a difficult control problem exhibiting sensor/actuator noncollocation has provided an irresistible allure for many researchers. The literature of the field continues to grow, and recent overviews of the problem are provided by Book (1993a, 1993b) and Canudas de Wit, Siciliano, and Bastin (1996).

The basic problem of controlling the endpoint motion using joint-based actuation can be divided into feedforward and feedback design, both of which are greatly complicated by the noncollocated nature of the relevant output. It is well known that the inverse dynamics problem typically leads to noncausal solutions (Bayo et al. 1989), and the relevant input-output map used in feedback design is nonminimum phase (De Luca, Lucibello, and Ulivi 1989). However, the torque to joint rate dynamics retain the favorable passivity property of the rigid situation. This key property is characteristic of systems with collocated dual actuation and sensing and underlies many of the known results for control of rigid robots (Canudas de Wit, Siciliano, and Bastin 1996). In this light, it has been suggested by De Luca and Siciliano (1993) that the endpoint problem be addressed indirectly using joint-based techniques that seek tracking of prescribed joint-space trajectories. An interesting compromise approach by Paden et al. (1993) used a causal approximation for the endpoint inverse dynamics solution in conjunction with a passive joint-based feedback.

Given the desirability of the minimum phase property or the stronger passivity property, several researchers have participated in the hunt for modified inputs and/or outputs that yield these properties. The reflected tip position was introduced by Wang and Vidyasagar (1990, 1992) for a single flexible link, and its rate was shown to yield a passivity property by Pota and Vidyasagar (1991). De Luca, Lucibello, and Ulivi (1989) showed that by using a suitable point along a single link as the output, minimum phase behavior could be obtained. Yim (1993) showed that this idea could work for a spatial three-link arm in which the last link is flexible. Barbieri (1993) analyzed the properties of transfer functions for various outputs in the single-link case. The possibility of transmitting the input torque to another location along a beam has been considered by Park and Asada (1994).

Among the reasons for designing a flexible robot arm are the desire for increased speed of operation, reduced robot mass as in space operations, and increased payload capability. The asymptotic situation of a large payload/robot mass ratio has been addressed by Damaren (1995), in which it was shown that the modified output idea could be used to obtain passivity for a general multilink flexible robot. This emanates from the clamped nature of the vibration modes at the manipulator end-effector. It was shown in Damaren (1996b) that feedforward design was possible that preserved the passivity property in the error dynamics, which opened the door to an adaptive approach (Damaren 1996a). These

The International Journal of Robotics Research,
Vol. 17, No. 6, June 1998, pp. 667–678,

analyses naturally lead to consideration of other systems that may enjoy similar properties.

In the present paper, we address planar two-link flexible manipulators and illustrate how the mass distribution in the links, joint stators, joint rotors, and payload affect the input-output map. The control problem for such a system was first addressed by Book, Maizza-Neto, and Whitney (1975) using classical approaches. Our key result shows that when the tip mass of each link is much greater than that of the link mass, certain modal properties greatly simplify feedforward and feedback design. Although the system is nonlinear, our philosophy is to examine the vibration modes for a generic configuration and infer potential control schemes for the actual system. This modal approach is later justified using a nonlinear model, and our numerical results indicate that good performance can be achieved using the proposed controllers.

Although the two-link scenario may seem unduly restrictive, it is a significant step forward from previous works that have emphasized either one-link or systems with one flexible link. Furthermore, many experimental systems that have been designed to study the efficacy of various control schemes fall into the two-link category. Our results may aid in interpreting the results produced by these facilities, many of which are constructed with flimsy links so as to be mass dominated by the motors and payload. In fact, the results of this paper were inspired by the initial examination by Damaren, Stanway, and Sharf (1995) of the modal properties of such a facility developed at the University of Victoria. Finally, insightful analytical progress and literal results are possible in the two-link case.

2. Motion Equations and Modal Analysis

The motion equation for flexible-link robots (omitting structural damping) can be written as

$$\mathbf{M}(\mathbf{q})\ddot{\mathbf{q}} + \mathbf{K}\mathbf{q} = [\mathbf{1}\ \ \mathbf{O}]^T\boldsymbol{\tau} + \mathbf{f}_{non}(\mathbf{q}, \dot{\mathbf{q}}), \tag{1}$$

where $\mathbf{M}$, $\mathbf{K}$, and $\boldsymbol{\tau}$ are the mass matrix, stiffness matrix, and joint torques, respectively. The nonlinear inertial forces $\mathbf{f}_{non}$ are quadratic in $\dot{\mathbf{q}}$. The generalized coordinates are partitioned as $\mathbf{q} = \text{col}\{\boldsymbol{\theta}, \mathbf{q}_e\}$, where $\boldsymbol{\theta}(t)$ are the N joint angles and $\mathbf{q}_e(t)$ are the N_e elastic coordinates. The latter are generated using clamped-free modeling for the elastic deflections of each link. Hence, the above matrices can be partitioned consistent with $\mathbf{q}$:

$$\mathbf{M} = \begin{bmatrix} \mathbf{M}_{\theta\theta} & \mathbf{M}_{\theta e} \\ \mathbf{M}_{\theta e}^T & \mathbf{M}_{ee} \end{bmatrix}, \quad \mathbf{K} = \begin{bmatrix} \mathbf{O} & \mathbf{O} \\ \mathbf{O} & \mathbf{K}_{ee} \end{bmatrix}, \tag{2}$$

with $\mathbf{M} = \mathbf{M}^T > \mathbf{O}$ and $\mathbf{K}_{ee} = \mathbf{K}_{ee}^T > \mathbf{O}$.

The kinematics describing the Cartesian end-effector displacements $\boldsymbol{\rho}(t)$ can be summarized by the forward kinematics map $\boldsymbol{\rho} = \boldsymbol{\mathcal{F}}(\boldsymbol{\theta}, \mathbf{q}_e)$, with $\dot{\boldsymbol{\rho}} = \mathbf{J}_\theta(\boldsymbol{\theta}, \mathbf{q}_e)\dot{\boldsymbol{\theta}} + \mathbf{J}_e(\boldsymbol{\theta}, \mathbf{q}_e)\dot{\mathbf{q}}_e$; $\mathbf{J}_\theta$ and $\mathbf{J}_e$ are Jacobian matrices. For the planar two-link manipulators considered here, $\boldsymbol{\rho} = [x\ \ y]^T$, where x and y are in-plane translations. A more general output known as the μ-tip rate has been defined by Damaren (1995):

$$\mathbf{y}(t) = \dot{\boldsymbol{\rho}}_\mu \triangleq \mathbf{J}_\theta\dot{\boldsymbol{\theta}} + \mu\mathbf{J}_e\dot{\mathbf{q}}_e, \tag{3}$$

where $\mu = 1$ captures the true tip rates and $\mu = 0$ constitutes an output involving only joint motions. For the duration of this paper, it is assumed that $\mathbf{J}_\theta$ is square and invertible. Given this assumption, a more useful control input for our purposes is $\mathbf{u}(t) \triangleq \mathbf{J}_\theta^{-T}\boldsymbol{\tau}$.

Consider small excursions of the coordinates $\delta\mathbf{q}$ in the vicinity of a constant configuration $\bar{\mathbf{q}} = \text{col}\{\bar{\boldsymbol{\theta}}, \mathbf{0}\}$. The linearized forms of eqs. (1) and (3) are

$$\begin{aligned} \mathbf{y} &= \mathbf{C}(\bar{\mathbf{q}})\delta\dot{\mathbf{q}} \quad \mathbf{M}(\bar{\mathbf{q}})\delta\ddot{\mathbf{q}} + \mathbf{K}\delta\mathbf{q} = \mathbf{B}(\bar{\mathbf{q}})\mathbf{u}(t) \\ \mathbf{u}(t) &= \mathbf{J}_\theta^{-T}(\bar{\mathbf{q}})\boldsymbol{\tau}(t), \end{aligned} \tag{4}$$

where the input and output matrices are $\mathbf{B}(\bar{\mathbf{q}}) = [\mathbf{J}_\theta\ \ \mathbf{O}]^T$ and $\mathbf{C}(\bar{\mathbf{q}}) = [\mathbf{J}_\theta\ \ \mu\mathbf{J}_e]$, respectively. The eigenproblem corresponding to (4) can be written as

$$-\omega_\alpha^2\mathbf{M}(\bar{\mathbf{q}})\mathbf{q}_\alpha + \mathbf{K}\mathbf{q}_\alpha = \mathbf{0}, \tag{5}$$

where ω_α are the unconstrained (joints unlocked) vibration frequencies and $\mathbf{q}_\alpha = \text{col}\{\boldsymbol{\theta}_\alpha, \mathbf{q}_{e\alpha}\}$, $\alpha = 1 \cdots N_e$, are the eigenvectors (mode shapes). Note that $\boldsymbol{\theta}_\alpha$ are the mode slopes at each joint axis. The term unconstrained is justified because each "clamped" link is embedded within a freely rotating frame. For a single-link system, the results of (5) would be the pinned-free modes whose motion ($\mathbf{q}_\alpha \cos\omega_\alpha t$) is composed of the clamped-free link deflections ($\mathbf{q}_{e\alpha} \cos\omega_\alpha t$) superimposed on the joint motion ($\boldsymbol{\theta}_\alpha \cos\omega_\alpha t$). In general, unconstrained modes are configuration dependent, whereas the constrained basis used for each link is not. This, coupled with the simple structure of the input matrix in (1) and (4), forms most of the motivation for this modeling approach.

Assuming N joints, there are also N zero-frequency rigid modes collectively of the form $\mathbf{Q}_r = [\mathbf{1}\ \ \mathbf{O}]^T$. The modes enjoy standard orthonormality relations with respect to $\mathbf{M}$ and $\mathbf{K}$:

$$\mathbf{q}_\alpha^T\mathbf{M}\mathbf{q}_\beta = \delta_{\alpha\beta} \qquad \mathbf{q}_\alpha^T\mathbf{M}\mathbf{Q}_r = \mathbf{O} \tag{6}$$

$$\mathbf{q}_\alpha^T\mathbf{K}\mathbf{q}_\beta = \omega_\alpha^2\delta_{\alpha\beta} \quad \mathbf{q}_\alpha^T\mathbf{K}\mathbf{Q}_r = \mathbf{O} \quad \alpha, \beta = 1 \cdots N_e. \tag{7}$$

Expanding the solution of eq. (4) in terms of eigenvectors $\delta\mathbf{q}(t) = \mathbf{Q}_r\boldsymbol{\eta}_r(t) + \sum_\alpha \mathbf{q}_\alpha\eta_\alpha(t)$, it is relatively straightforward to obtain the modal equations

$$\mathbf{y} = \mathbf{J}_\theta\dot{\boldsymbol{\eta}}_r + \sum_{\alpha=1}^{N_e}(\mathbf{J}_\theta\boldsymbol{\theta}_\alpha + \mu\mathbf{J}_e\mathbf{q}_{e\alpha})\dot{\eta}_\alpha$$

$$\mathbf{M}_{\theta\theta}\ddot{\boldsymbol{\eta}}_r = \boldsymbol{\tau}(t) = \mathbf{J}_\theta^T\mathbf{u} \tag{8}$$

$$\ddot{\eta}_\alpha + \omega_\alpha^2\eta_\alpha = (\mathbf{J}_\theta\boldsymbol{\theta}_\alpha)^T\mathbf{u}(t), \quad \alpha = 1 \cdots N_e. \tag{9}$$

Using Laplace transforms, the dynamics of the linearized system can be captured by the input-output description

$$\mathbf{y}(s) = \mathbf{G}(s)\mathbf{u}(s) \tag{10}$$

$$\mathbf{G}(s) = \frac{1}{s}\mathbf{J}_\theta \mathbf{M}_{\theta\theta}^{-1}\mathbf{J}_\theta^T + \sum_{\alpha=1}^{N_e} \frac{s}{s^2+\omega_\alpha^2}\mathbf{c}_\alpha \mathbf{b}_\alpha^T \tag{11}$$

$$\mathbf{c}_\alpha = \mathbf{C}\mathbf{q}_\alpha = \mathbf{J}_\theta \boldsymbol{\theta}_\alpha + \mu \mathbf{J}_e \mathbf{q}_{e\alpha}\,,$$

$$\mathbf{b}_\alpha = \mathbf{B}^T\mathbf{q}_\alpha = \mathbf{J}_\theta \boldsymbol{\theta}_\alpha. \tag{12}$$

Many important properties of this system are governed by the relationship between $\mathbf{b}_\alpha$ and $\mathbf{c}_\alpha$.

Recall that a general square system is passive if $\int_0^T \mathbf{y}^T\mathbf{u}\,dt \geq 0$, $\forall T \geq 0$, and $\forall \mathbf{u}$ such that $\int_0^T \mathbf{u}^T\mathbf{u}\,dt < \infty$. For linear time-invariant systems, this is equivalent to positive realness of the corresponding transfer function $\mathbf{G}(s)$; that is, $\mathbf{G}(s)$ is analytic, and $\mathbf{G}(s) + \mathbf{G}^H(s) \geq \mathbf{O}$ for s in the open right-half plane. The major significance of the passivity property is the closed-loop stabilization predicted by the passivity theorem (Desoer and Vidyasagar 1975); that is, a strictly passive controller such as a PI law (a PD law applied to position) will stabilize a passive plant.

Following Newcomb (1966) and Anderson and Vongpanitlerd (1973), a transfer matrix of the form $\mathbf{G}(s)$ in (11) is positive real if and only if $\mathbf{c}_\alpha\mathbf{b}_\alpha^T \geq \mathbf{O}$, since the coefficient of s^{-1} is nonnegative definite. The easiest way for this to happen is $\mathbf{c}_\alpha = \mathbf{b}_\alpha$, which is ensured when $\mathbf{C} = \mathbf{B}^T$; that is, collocation of actuation and rate sensing. Among the first to recognize the relative ease with which such a system could be stabilized was Gevarter (1970), who showed by using perturbation arguments that small proportional and derivative gains were stabilizing in the collocated case. A specific instance of this occurs when $\mu = 0$, which implies that $\mathbf{y} = \mathbf{J}_\theta\dot{\boldsymbol{\theta}}$ and $\mathbf{b}_\alpha = \mathbf{c}_\alpha = \mathbf{J}_\theta\boldsymbol{\theta}_\alpha$.

An important question then arises: Is collocation the only mechanism by which $\mathbf{c}_\alpha\mathbf{b}_\alpha^T \geq \mathbf{O}$? In the SISO case, this is somewhat easier to achieve, since $c_\alpha b_\alpha > 0$ only requires that c_α and b_α have the same sign. In general, for $\mu \neq 0$, the vectors $\mathbf{b}_\alpha$ and $\mathbf{c}_\alpha$ will not resemble each other, which reflects noncollocation of the joint actuation and end-effector rate sensing. In Damaren (1995), it was shown that if a nonredundant flexible manipulator carries a payload much more massive than the arm, then $\mathbf{J}_\theta\boldsymbol{\theta}_\alpha + \mathbf{J}_e\mathbf{q}_{e\alpha} \doteq \mathbf{0}$; that is, the mode shapes are approximately clamped at the end-effector. In this case, the input-output map from torques to end-effector rates becomes essentially rigid, since the vibration modes become unobservable from the tip. This follows from $\mathbf{c}_\alpha \doteq \mathbf{0}$ in (11). Furthermore, for general μ, $\mathbf{c}_\alpha\mathbf{b}_\alpha^T \doteq (1-\mu)(\mathbf{J}_\theta\boldsymbol{\theta}_\alpha)(\mathbf{J}_\theta\boldsymbol{\theta}_\alpha)^T$, which is nonnegative definite if $\mu \leq 1$, thus rendering the transfer matrix in (11) positive real. Other ramifications of this property will be discussed in Section 5.

In the interest of finding other situations in which this key property holds, we note the following result.

LEMMA 1. The mode shapes, $\mathbf{q}_\alpha$, of (5) satisfy $\mathbf{J}_\theta\boldsymbol{\theta}_\alpha + \mathbf{J}_e\mathbf{q}_{e\alpha} = \mathbf{0}$, $\alpha = 1 \cdots N_e$, if and only if $\mathbf{M}_{\theta\theta}\mathbf{J}_\theta^{-1}\mathbf{J}_e = \mathbf{M}_{\theta e}$.

Proof. Using the eigenequation (5) and the partitioning of the mass and stiffness matrices in (2), the eigencolumns satisfy $\mathbf{M}_{\theta\theta}\boldsymbol{\theta}_\alpha + \mathbf{M}_{\theta e}\mathbf{q}_{e\alpha} = \mathbf{0}$. Thus,

$$\begin{aligned}\mathbf{J}_\theta\boldsymbol{\theta}_\alpha + \mathbf{J}_e\mathbf{q}_{e\alpha} &= \mathbf{J}_\theta(\boldsymbol{\theta}_\alpha + \mathbf{J}_\theta^{-1}\mathbf{J}_e\mathbf{q}_{e\alpha}) \\ &= \mathbf{J}_\theta\mathbf{M}_{\theta\theta}^{-1}(\mathbf{M}_{\theta\theta}\mathbf{J}_\theta^{-1}\mathbf{J}_e - \mathbf{M}_{\theta e})\mathbf{q}_{e\alpha}.\end{aligned}$$

Clearly, we have sufficiency. Suppose $\mathbf{J}_\theta\boldsymbol{\theta}_\alpha + \mathbf{J}_e\mathbf{q}_{e\alpha} = \mathbf{0}$. Since N_e $\mathbf{q}_{e\alpha}$ are linearly independent, the null space of the $N \times N_e$ matrix $(\mathbf{M}_{\theta\theta}\mathbf{J}_\theta^{-1}\mathbf{J}_e - \mathbf{M}_{\theta e})$ must have dimension N_e; hence, $\mathbf{M}_{\theta\theta}\mathbf{J}_\theta^{-1}\mathbf{J}_e - \mathbf{M}_{\theta e} = \mathbf{O}$. □

In the next section, the existence of this property for planar two-link manipulators will be addressed. Note that this necessary and sufficient condition is independent of the stiffness properties.

3. Main Results: Two-Link Flexible Manipulators

Consider the arm in Figure 1. Let $m_{\ell n}$ and ℓ_n denote the mass and length of the uniform elastic link and define $\rho_n = m_{\ell n}/\ell_n$, $n = 1, 2$. At the end of each link is a tip mass with mass m_{tn} and inertia J_{tn}. At each joint is a rotor with mass m_{rn} and inertia J_{rn}.

Denote the reference frames in Figure 1 by $\mathcal{F}_n$ and $\mathcal{F}_{tn}$, $n = 1, 2$, and let $\mathbf{v}_n = [v_{nx}\ v_{ny}\ \omega_{nz}]^T$ denote the generalized velocity of $\mathcal{F}_n$; that is, v_{nx} and v_{ny} are the absolute velocity components of $\mathcal{F}_n$ expressed in $\mathcal{F}_n$, and ω_{nz} is the absolute angular velocity. The velocity of $\mathcal{F}_{tn}$, $\mathbf{v}_{tn}$ is defined similarly. The transverse elastic deformation of each link is designated $u_{ne}(x_n, t)$ and expressed as

$$u_{ne}(x_n, t) = \sum_{\beta=1}^{N_{ne}} \psi_{n\beta}(x_n)q_{n\beta}(t), \tag{13}$$

where the $\psi_{n\beta}$ are cantilevered shape functions. We define the following matrix quantities:

$$\begin{aligned}&\boldsymbol{\Psi}_n = row\{\psi_{n\beta}(\ell_n)\} \quad \boldsymbol{\Phi}_n = row\{\psi'_{n\beta}(\ell_n)\} \\ &\mathbf{q}_{ne} = col\{q_{n\beta}(t)\}\end{aligned} \tag{14}$$

Also,

$$\mathbf{P}_n = row\{P_{n\beta}\} \quad \mathbf{H}_n = row\{H_{n\beta}\}, \tag{15}$$

where

$$P_{n\beta} = \rho_n \int_0^{\ell_n} \psi_{n\beta}(x_n)\,dx_n$$

and

$$H_{n\beta} = \rho_n \int_0^{\ell_n} x_n\psi_{n\beta}(x_n)\,dx_n$$

are the momentum coefficients.

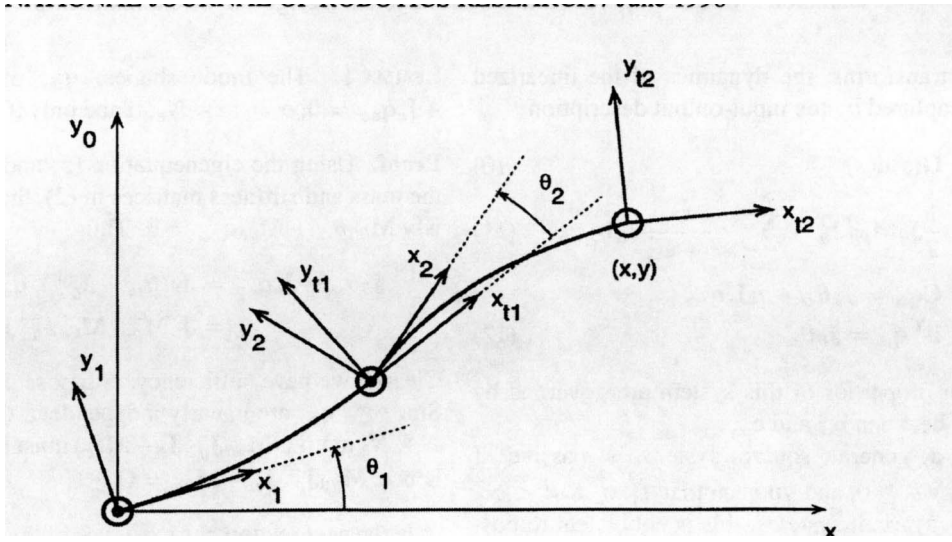

Fig. 1. Two-link manipulator.

With these definitions, it is straightforward to show that

$$\mathbf{v}_1 = \begin{bmatrix} 0 \\ 0 \\ 1 \end{bmatrix} \dot{\theta}_1 \quad \mathbf{v}_{t1} = \begin{bmatrix} 0 \\ \ell_1 \\ 1 \end{bmatrix} \dot{\theta}_1 + \begin{bmatrix} 0 \\ \Psi_1 \\ \Phi_1 \end{bmatrix} \dot{\mathbf{q}}_{e1} \quad (16)$$

$$\mathbf{v}_2 = \begin{bmatrix} -\ell_1 s_2 & 0 \\ \ell_1 c_2 & 0 \\ 1 & 1 \end{bmatrix} \begin{bmatrix} \dot{\theta}_1 \\ \dot{\theta}_2 \end{bmatrix} + \begin{bmatrix} -s_2 \Psi_1 \\ c_2 \Psi_1 \\ \Phi_1 \end{bmatrix} \dot{\mathbf{q}}_{e1} \quad (17)$$

$$\mathbf{v}_{t2} = \begin{bmatrix} -\ell_1 s_2 & 0 \\ \ell_1 c_2 + \ell_2 & \ell_2 \\ 1 & 1 \end{bmatrix} \begin{bmatrix} \dot{\theta}_1 \\ \dot{\theta}_2 \end{bmatrix} + \begin{bmatrix} -s_2 \Psi_1 & \mathbf{0} \\ c_2 \Psi_1 + \ell_2 \Phi_1 & \Psi_2 \\ \Phi_1 & \Phi_2 \end{bmatrix} \begin{bmatrix} \dot{\mathbf{q}}_{e1} \\ \dot{\mathbf{q}}_{e2} \end{bmatrix}, \quad (18)$$

where $s_n = \sin\theta_n$, $c_n = \cos\theta_n$. The last expression furnishes the Jacobian matrices $\mathbf{J}_\theta = \mathbf{C}_{02}\hat{\mathbf{J}}_\theta$, $\mathbf{J}_e = \mathbf{C}_{02}\hat{\mathbf{J}}_e$ with

$$\hat{\mathbf{J}}_\theta = \begin{bmatrix} -\ell_1 s_2 & 0 \\ \ell_1 c_2 + \ell_2 & \ell_2 \end{bmatrix} \quad \hat{\mathbf{J}}_e = \begin{bmatrix} -s_2 \Psi_1 & \mathbf{0} \\ c_2 \Psi_1 + \ell_2 \Phi_1 & \Psi_2 \end{bmatrix}$$
$$\mathbf{C}_{02} = \begin{bmatrix} c_{12} & -s_{12} \\ s_{12} & c_{12} \end{bmatrix}, \quad (19)$$

where $c_{12} = \cos(\theta_1 + \theta_2)$ and $s_{12} = \sin(\theta_1 + \theta_2)$. The above expressions have been linearized in the elastic variables in anticipation of the eigenproblem discussed in the previous section. The exact versions of eqs. (16)-(19) would account for the elastic displacement and rotation of the end of each link in forming the various coordinate transformations.

The kinetic energy of the tip masses is given by

$$T_{tip} = \tfrac{1}{2} \sum_{n=1}^{2} \mathbf{v}_{tn}^T \mathbf{M}_{tip,n} \mathbf{v}_{tn},$$
$$\mathbf{M}_{tip,n} = diag\{m_{tn}, m_{tn}, J_{tn}\}. \quad (20)$$

For the links, we have

$$T_{lnk} = \tfrac{1}{2} \sum_{n=1}^{2} \left(\mathbf{v}_n^T \mathbf{M}_{lnk,n} \mathbf{v}_n + 2\dot{\mathbf{q}}_{ne}^T \begin{bmatrix} \mathbf{0} & \mathbf{P}_n^T & \mathbf{H}_n^T \end{bmatrix} \mathbf{v}_n + \dot{\mathbf{q}}_{ne}^T \mathbf{M}_{n,ee} \dot{\mathbf{q}}_{ne} \right) \quad (21)$$

$$\mathbf{M}_{lnk,n} = m_{\ell n} \begin{bmatrix} 1 & 0 & 0 \\ 0 & 1 & \ell_n/2 \\ 0 & \ell_n/2 & \ell_n^2/3 \end{bmatrix}$$

$$\mathbf{M}_{n,ee} = \underset{\alpha,\beta}{matrix} \left\{ \rho_n \int_0^{\ell_n} \psi_{n\alpha}(x_n) \psi_{n\beta}(x_n)\, dx_n \right\}, \quad (22)$$

and for the rotors,

$$T_{rot} = \tfrac{1}{2} \sum_{n=1}^{2} \mathbf{v}_n^T \mathbf{M}_{rot,n} \mathbf{v}_n$$
$$\mathbf{M}_{rot,n} = diag\{m_{rn}, m_{rn}, J_{rn}\}. \quad (23)$$

Using these in conjunction with the velocity expressions in (16)-(18) allows us to extract the corresponding contributions to the mass matrices $\mathbf{M}_{\theta\theta}$ and $\mathbf{M}_{\theta e}$ in (2).

Writing $\mathbf{M}_{\theta\theta} = \mathbf{M}_{\theta\theta}^{(tip)} + \mathbf{M}_{\theta\theta}^{(lnk)} + \mathbf{M}_{\theta\theta}^{(rot)}$, with a similar decomposition for $\mathbf{M}_{\theta e}$, we have the following results:

$$\mathbf{M}_{\theta\theta}^{(tip)} = \begin{bmatrix} (m_{t1} + m_{t2})\ell_1^2 + 2m_{t2}\ell_1\ell_2 c_2 + m_{t2}\ell_2^2 + J_{t1} + J_{t2} & m_{t2}\ell_2(\ell_1 c_2 + \ell_2) + J_{t2} \\ m_{t2}\ell_2(\ell_1 c_2 + \ell_2) + J_{t2} & m_{t2}\ell_2^2 + J_{t2} \end{bmatrix} \quad (24)$$

$$\mathbf{M}_{\theta\theta}^{(tip)} \mathbf{J}_\theta^{-1} \mathbf{J}_e = \begin{bmatrix} ((m_{t1} + m_{t2})\ell_1 + m_{t2}\ell_1 c_2)\Psi_1 + m_{t2}(\ell_2 + \ell_1 c_2)\ell_2 \Phi_1 & m_{t2}(\ell_2 + \ell_1 c_2)\Psi_2 \\ m_{t2}\ell_2(c_2 \Psi_1 + \ell_2 \Phi_1) & m_{t2}\ell_2 \Psi_2 \end{bmatrix}$$

$$+\begin{bmatrix} J_{t1}\ell_1^{-1}\Psi_1 + J_{t2}\Phi_1 & J_{t2}\ell_2^{-1}\Psi_2 \\ J_{t2}\Phi_1 & J_{t2}\ell_2^{-1}\Psi_2 \end{bmatrix} \quad (25)$$

$$\mathbf{M}_{\theta e}^{(tip)} = \begin{bmatrix} ((m_{t1}+m_{t2})\ell_1 & m_{t2}(\ell_2 \\ +m_{t2}\ell_1 c_2)\Psi_1 & +\ell_1 c_2)\Psi_2 \\ +m_{t2}(\ell_2+\ell_1 c_2)\ell_2\Phi_1 & \\ m_{t2}\ell_2(c_2\Psi_1+\ell_2\Phi_1) & m_{t2}\ell_2\Psi_2 \end{bmatrix}$$

$$+\begin{bmatrix} (J_{t1}+J_{t2})\Phi_1 & J_{t2}\Phi_2 \\ J_{t2}\Phi_1 & J_{t2}\Phi_2 \end{bmatrix} \quad (26)$$

$$\mathbf{M}_{\theta\theta}^{(lnk)} = \begin{bmatrix} (m_{\ell 1}+3m_{\ell 2})\ell_1^2/3 & m_{\ell 2}\ell_1\ell_2 c_2/2 \\ +m_{\ell 2}\ell_1\ell_2 c_2 & +m_{\ell 2}\ell_2^2/3 \\ +m_{\ell 2}\ell_2^2/3 & \\ m_{\ell 2}\ell_1\ell_2 c_2/2 & \\ +m_{\ell 2}\ell_2^2/3 & m_{\ell 2}\ell_2^2/3 \end{bmatrix} \quad (27)$$

$$\mathbf{M}_{\theta\theta}^{(lnk)}\mathbf{J}_\theta^{-1}\mathbf{J}_e = \begin{bmatrix} m_{\ell 2}(\ell_1 & \\ +\ell_2 c_2/2)\Psi_1 & m_{\ell 2}(\ell_2/3)\Psi_2 \\ +m_{\ell 2}(\ell_2/6)(2\ell_2 & +m_{\ell 1}c_2(\ell_1/2)\Psi_2 \\ +3\ell_1 c_2)\Psi_1 & \\ +m_{\ell 1}(\ell_1/3)\Psi_1 & \\ m_{\ell 2}(\ell_2/6)(3c_2\Psi_1 & \\ +2\ell_2\Psi_1) & m_{\ell 2}(\ell_2/3)\Psi_2 \end{bmatrix} \quad (28)$$

$$\mathbf{M}_{\theta e}^{(lnk)} = \begin{bmatrix} m_{\ell 2}(\ell_1+\ell_2 c_2/2)\Psi_1 & \mathbf{H}_2 + c_2\ell_1\mathbf{P}_2 \\ +m_{\ell 2}(\ell_2/6)(2\ell_2 & \\ +3\ell_1 c_2)\Psi_1 + \mathbf{H}_1 & \\ m_{\ell 2}(\ell_2/6)(3c_2\Psi_1 & \\ +2\ell_2\Psi_1) & \mathbf{H}_2 \end{bmatrix} \quad (29)$$

$$\mathbf{M}_{\theta\theta}^{(rot)} = \begin{bmatrix} J_{r1}+J_{r2}+m_{r2}\ell_1^2 & J_{r2} \\ J_{r2} & J_{r2} \end{bmatrix} \quad (30)$$

$$\mathbf{M}_{\theta\theta}^{(rot)}\mathbf{J}_\theta^{-1}\mathbf{J}_e = \begin{bmatrix} m_{r2}\ell_1\Psi_1 + J_{r2}\Phi_1 & J_{r2}\ell_2^{-1}\Psi_2 \\ +J_{r1}\ell_1^{-1}\Psi_1 & \\ J_{r2}\Phi_1 & J_{r2}\ell_2^{-1}\Psi_2 \end{bmatrix} \quad (31)$$

$$\mathbf{M}_{\theta e}^{(rot)} = \begin{bmatrix} m_{r2}\ell_1\Psi_1 + J_{r2}\Phi_1 & \mathbf{0} \\ J_{r2}\Phi_1 & \mathbf{0} \end{bmatrix}. \quad (32)$$

Some general comments regarding these expressions are in order. First, when $J_{t1} = J_{t2} = 0$, the tip quantities given by (25) and (26) produce the momentum balance required in Lemma 1. When $J_{tn} \neq 0$, these expressions are equal if $\Psi_n = \ell_n\Phi_n$. Second, the link quantities in (28) and (29) are also equal if $2\mathbf{P}_n = m_{\ell n}\Psi_n$ and $3\mathbf{H}_n = m_{\ell n}\ell_n\Psi_n$. These conditions will not be satisfied in general. For example, for the first cantilevered-free mode shape of a uniform beam, $\psi_{n1} \doteq 0.726\ell_n\theta_{n1}$, $2.56P_{n1} \doteq m_{\ell n}\psi_{n1}$, and $3.52H_{n1} \doteq m_{\ell n}\ell_n\psi_{n1}$. However, there is one important situation addressed below in Lemma 2 in which they do hold. In general, the rotor terms in (31) and (32) do not constitute the required balance. As expected, the contributions of m_{r2} mirror those of m_{t1}, and it will be assumed that they have been incorporated into the latter.

LEMMA 2. Assume that $J_{r1} = J_{r2} = 0$, and that each link is modeled by a single linear shape function $\psi_{n1} = C_n x_n$, where C_n is a normalization constant. Then,

$$\mathbf{J}_\theta\boldsymbol{\theta}_\alpha + \mathbf{J}_e\mathbf{q}_{e\alpha} = \mathbf{0}\,, \quad \alpha = 1, 2$$

for all $m_{tn} > 0$, $m_{\ell n} > 0$, $J_{tn} > 0$, and $\bar{\theta}_2 \in (0, \pi)$.

Proof. Since $\Psi_n = \psi_{n1}(\ell_n) = C_n\ell_n$, we have $\Phi_n = C_n = \ell_n^{-1}\Psi_n$, $\mathbf{P}_n = (m_{\ell n}/2)\Psi_n$, and $\mathbf{H}_n = (m_{\ell n}\ell_n/3)\Psi_n$. Hence, on the basis of (25)-(29), $(\mathbf{M}_{\theta\theta}^{(tip)} + \mathbf{M}_{\theta\theta}^{(lnk)})\mathbf{J}_\theta^{-1}\mathbf{J}_e = (\mathbf{M}_{\theta e}^{(tip)} + \mathbf{M}_{\theta e}^{(lnk)})$, from which the result follows using Lemma 1. □

Note that this situation corresponds precisely to a flexible-joint robot with lumped torsional stiffnesses at the link roots and rotors of vanishingly small moment of inertia. Next, we examine the situation for a more realistic discretization strategy.

DEFINITION 1.

$$\mathrm{J}_\alpha \triangleq \frac{\|\boldsymbol{\rho}_\alpha\|}{\|\mathbf{J}_\theta\boldsymbol{\theta}_\alpha\|}\,, \quad \boldsymbol{\rho}_\alpha \triangleq \mathbf{J}_\theta\boldsymbol{\theta}_\alpha + \mathbf{J}_e\mathbf{q}_{e\alpha}, \quad (33)$$

where $\|(\cdot)\|$ denotes the Euclidean norm.

THEOREM 1. Let $m_{\ell 1}/m_{\ell 2} = C_\ell$, $m_{t1}/m_{t2} = C_t$ and $\epsilon_2 = m_{\ell 2}/m_{t2}$, and assume that $J_{tn} = J_{rn} = 0$, $n = 1, 2$. Then, J_α is $\mathcal{O}(\epsilon_2)$, $\alpha = 1 \cdots N_e$, for $\bar{\theta}_2 \in (0, \pi)$.

Proof. Begin by nondimensionalizing modal quantities as follows: $\hat{\Psi}_n = \sqrt{m_{\ell n}}\Psi_n$, $\hat{\Phi}_n = \Phi_n\sqrt{m_{\ell n}}/\ell_n$, $\hat{\mathbf{P}}_n = (\sqrt{m_{\ell n}})^{-1}\mathbf{P}_n$, $\hat{\mathbf{H}}_n = (\sqrt{m_{\ell n}}\ell_n)^{-1}\mathbf{H}_n$. Using the expressions in (25)-(29),

$$(\mathbf{M}_{\theta\theta}\mathbf{J}_\theta^{-1}\mathbf{J}_e - \mathbf{M}_{\theta e})\mathbf{q}_{e\alpha} = \begin{bmatrix} (m_{\ell 1}\ell_1/3)\Psi_1 - \mathbf{H}_1 & (m_{\ell 2}\ell_2/3)\Psi_2 - \mathbf{H}_2 \\ & +\ell_1 c_2((m_{\ell 2}/2)\Psi_2 - \mathbf{P}_2) \\ \mathbf{0} & (m_{\ell 2}\ell_2/3)\Psi_2 - \mathbf{H}_2 \end{bmatrix}\mathbf{q}_{e\alpha}$$

$$= \sqrt{m_{\ell 2}}\underbrace{\begin{bmatrix} \sqrt{C_\ell}\ell_1(\frac{1}{3}\hat{\Psi}_1 - \hat{\mathbf{H}}_1) & \ell_2(\frac{1}{3}\hat{\Psi}_2 - \hat{\mathbf{H}}_2) \\ & +\ell_1 c_2(\frac{1}{2}\hat{\Psi}_2 - \hat{\mathbf{P}}_2) \\ \mathbf{0} & \ell_2(\frac{1}{3}\hat{\Psi}_2 - \hat{\mathbf{H}}_2) \end{bmatrix}}\mathbf{q}_{e\alpha}$$

$$\triangleq \sqrt{m_{\ell 2}}\tilde{\mathbf{M}}_{\theta e}\mathbf{q}_{e\alpha}.$$

Noting that $\boldsymbol{\rho}_\alpha = \mathbf{J}_\theta\mathbf{M}_{\theta\theta}^{-1}(\mathbf{M}_{\theta\theta}\mathbf{J}_\theta^{-1}\mathbf{J}_e - \mathbf{M}_{\theta e})\mathbf{q}_{e\alpha}$ and writing $\widehat{\mathbf{M}}_{\theta\theta} = m_{t2}^{-1}\mathbf{M}_{\theta\theta}^{(tip)}$, we have

$$\begin{aligned} \lim_{\epsilon_2\to 0}\|\boldsymbol{\rho}_\alpha\| &\leq \lim_{\epsilon_2\to 0} m_{t2}^{-1}\bar{\sigma}(\mathbf{J}_\theta)\bar{\sigma}(\widehat{\mathbf{M}}_{\theta\theta}^{-1}) \\ &\quad \|(\mathbf{M}_{\theta\theta}\mathbf{J}_\theta^{-1}\mathbf{J}_e - \mathbf{M}_{\theta e})\mathbf{q}_{e\alpha}\| \\ &\leq \lim_{\epsilon_2\to 0} \epsilon_2\bar{\sigma}(\mathbf{J}_\theta)\bar{\sigma}(\widehat{\mathbf{M}}_{\theta\theta}^{-1})\bar{\sigma} \\ &\quad \times(\tilde{\mathbf{M}}_{\theta e})(\sqrt{m_{\ell 2}})^{-1}\|\mathbf{q}_{e\alpha}\|. \end{aligned} \quad (34)$$

Here, $\bar{\sigma}(\cdot)$ denotes the largest singular value. Given the normalization for $\mathbf{q}_\alpha$ in (6), $\|\mathbf{q}_{e\alpha}\|^2 \leq \|\mathbf{q}_\alpha\|^2 \leq \underline{\lambda}^{-1}(\mathbf{M})$, where $\underline{\lambda}(\cdot)$ is the smallest eigenvalue; hence, $\|\boldsymbol{\rho}_\alpha\| \to 0$ as $\epsilon_2 \to 0$, and the endpoint of the manipulator becomes a node for each vibration mode. Considering that $\mathbf{C}_{02}^T\boldsymbol{\rho}_\alpha = \hat{\mathbf{J}}_\theta\boldsymbol{\theta}_\alpha + \hat{\mathbf{J}}_e\mathbf{q}_{e\alpha} \to \mathbf{0}$ as well, (19) yields $-s_2(\ell_1\theta_{1\alpha} + \boldsymbol{\Psi}_1\mathbf{q}_{1e,\alpha}) \to 0$, and the endpoint of the first link also becomes a node for $s_2 \neq 0$. We conclude that the asymptotic behavior of each vibration mode corresponds to pinned-pinned motion for each link, and hence $\mathbf{q}_\alpha$ is independent of m_{t2}; that is, ϵ_2. Furthermore, $\boldsymbol{\theta}_\alpha \neq \mathbf{0}$, and $\mathbf{M}_{\theta e}\mathbf{q}_{e\alpha} = -\mathbf{M}_{\theta\theta}\boldsymbol{\theta}_\alpha \neq \mathbf{0}$.

Consider the denominator of J_α in (33). As $\epsilon_2 \to 0$,

$$\mathbf{M}_{\theta e}\mathbf{q}_{e\alpha} \to \mathbf{M}_{\theta e}^{(tip)}\mathbf{q}_{e\alpha}$$
$$= (m_{t2}/\sqrt{m_{\ell 2}}) \underbrace{\begin{bmatrix} ((1+C_t+c_2)\ell_1\hat{\Psi}_1 & (\ell_2+\ell_1 c_2)\hat{\Psi}_2 \\ +(\ell_2+\ell_1 c_2)\ell_2\ell_1\hat{\Phi}_1 & \\ \ell_2(c_2\hat{\Psi}_1+\ell_2\ell_1\hat{\Phi}_1) & \ell_2\hat{\Psi}_2 \end{bmatrix}}_{\frac{m_{t2}}{\sqrt{m_{\ell 2}}}\hat{\mathbf{M}}_{\theta e}\mathbf{q}_{e\alpha}} \mathbf{q}_{e\alpha}$$
$$\equiv \frac{m_{t2}}{\sqrt{m_{\ell 2}}}\hat{\mathbf{M}}_{\theta e}\mathbf{q}_{e\alpha}.$$

Hence, in the limit,

$$\|\mathbf{J}_\theta\boldsymbol{\theta}_\alpha\| = \|\mathbf{J}_\theta\mathbf{M}_{\theta\theta}^{-1}\mathbf{M}_{\theta e}\mathbf{q}_{e\alpha}\| \geq (\sqrt{m_{\ell 2}})^{-1}\underline{\sigma}(\mathbf{J}_\theta)\underline{\sigma}(\hat{\mathbf{M}}_{\theta\theta}^{-1})\|\hat{\mathbf{M}}_{\theta e}\mathbf{q}_{e\alpha}\|, \quad (35)$$

where $\underline{\sigma}(\cdot)$ is the least singular value. Combining this with (34) and noting the definition (33) gives

$$\lim_{\epsilon_2\to 0}\mathrm{J}_\alpha \leq \lim_{\epsilon_2\to 0}\frac{m_{\ell 2}}{m_{t2}}\frac{\bar{\sigma}(\mathbf{J}_\theta)\bar{\sigma}(\hat{\mathbf{M}}_{\theta\theta}^{-1})}{\underline{\sigma}(\mathbf{J}_\theta)\underline{\sigma}(\hat{\mathbf{M}}_{\theta\theta}^{-1})}\frac{\|\tilde{\mathbf{M}}_{\theta e}\mathbf{q}_{e\alpha}\|}{\|\hat{\mathbf{M}}_{\theta e}\mathbf{q}_{e\alpha}\|} = C\epsilon_2,$$

where C is independent of ϵ_2. This follows from the fact that $\mathbf{q}_{1e,\alpha}$ and $\mathbf{q}_{2e,\alpha}$ tend toward the "elastic part" of the pinned-pinned vibration mode and that the ratio of norms involving $\mathbf{q}_{e\alpha}$ is independent of normalization. □

Although the above result neglects the self-inertia of tip bodies and inboard rotors, the effect of the latter is somewhat mitigated. The discrepancies between (31) and (32) are of the form $J_{rn}\ell_n^{-1}\boldsymbol{\Psi}_n$, and therefore the first-order impact on $\boldsymbol{\rho}_\alpha$ is terms containing $\boldsymbol{\Psi}_n\mathbf{q}_{ne,\alpha}$. Given the pinned-pinned behavior of the modes discovered above, the first-order effect of J_{rn} is zero as $\epsilon_2 \to 0$. It is worth mentioning that none of the results given above relies on the elastic properties of the link, only on the interplay between kinematics and mass properties.

The reader may naturally wonder what happens beyond two links in the planar case. Consider the addition of a third link with corresponding properties $m_{\ell 3}$, ℓ_3, m_{t3}, J_{t3}, m_{r3}, and augmentation of $\boldsymbol{\rho}$ with the rotation of $\mathcal{F}_{t3}$ with respect to $\mathcal{F}_0$; that is, $\boldsymbol{\rho} = [x \;\; y \;\; \phi]^T$. The Jacobians corresponding to (19) are

$$\hat{\mathbf{J}}_\theta = \begin{bmatrix} -\ell_1 s_{23} - \ell_2 s_3 & -\ell_2 s_3 & 0 \\ \ell_1 c_{23} + \ell_2 c_3 + \ell_3 & \ell_2 c_3 + \ell_3 & \ell_3 \\ 1 & 1 & 1 \end{bmatrix}$$
$$\hat{\mathbf{J}}_e = \begin{bmatrix} -\Psi_1 s_{23} - \ell_2\Phi_1 s_3 & -\Psi_2 s_3 & \mathbf{0} \\ \Psi_1 c_{23} + (\ell_2 c_3 + \ell_3)\Phi_1 & c_3\Psi_2 + \ell_3\Phi_2 & \Psi_3 \\ \Phi_1 & \Phi_2 & \Phi_3 \end{bmatrix}.$$

Calculations analogous to (25) and (26) show that the required balance is now achieved for m_{t1} and m_{t2} if $\Psi_3 = \ell_3\Phi_3$. This is trivially accomplished if the third link is rigid. The balance occurs for J_{t1} and J_{t2} if $\Psi_n = \ell_n\Phi_n$, $n = 1, 2, 3$. Lemma 2 generalizes to the three-link case, since with $\psi_{n1} = x_n$ and $J_{rn} = 0$, $n = 1, 2, 3$, $\hat{\mathbf{J}}_\theta = \hat{\mathbf{J}}_e$ and $\mathbf{M}_{\theta\theta} = \mathbf{M}_{\theta e}$.

For m_{t3} and J_{t3}, the balance always occurs, since the contributions to $\mathbf{M}_{\theta\theta}^{(tip)}$ and $\mathbf{M}_{\theta e}^{(tip)}$ are $\hat{\mathbf{J}}_\theta^T\mathbf{M}_{tip,3}\hat{\mathbf{J}}_\theta$ and $\hat{\mathbf{J}}_\theta^T\mathbf{M}_{tip,3}\hat{\mathbf{J}}_e$, respectively, where $\mathbf{M}_{tip,3}$ is generated according to (20). This is expected given the large payload results of Damaren (1995). Furthermore, J_{t3} pervades all nine entries of the matrices $\mathbf{M}_{\theta e}^{(tip)}$ and $\mathbf{M}_{\theta\theta}^{(tip)}\mathbf{J}_\theta^{-1}\mathbf{J}_e$. With these observations, we permit the following extension of Theorem 1 for a planar three-link flexible manipulator with the third link rigid: if $J_{r1} = J_{r2} = 0$, then $\mathrm{J}_\alpha \to 0$, $\alpha = 1 \cdots N_e$, as $m_{\ell n}/m_{tn} \to 0$ and $J_{tn}/J_{t3} \to 0$, $n = 1, 2$. Here, J_α is the three-dimensional version of (33), and we assume as before that $\det \mathbf{J}_\theta \neq 0$. Unlike the two-link case, the tip inertias of links 1 and 2 need now only be small compared to the payload inertia J_{t3}.

4. Control System Design

The nonlinear consequences of the property $\mathbf{M}_{\theta\theta}\mathbf{J}_\theta^{-1}\mathbf{J}_e = \mathbf{M}_{\theta e}$ are easily deduced. Letting $\dot{\boldsymbol{\theta}} = \mathbf{J}_\theta^{-1}(\dot{\boldsymbol{\rho}} - \mathbf{J}_e\dot{\mathbf{q}}_e)$, the kinetic energy $T = \frac{1}{2}\dot{\mathbf{q}}^T\mathbf{M}\dot{\mathbf{q}}$ decouples into $T = T_\rho + T_e$, where

$$T_\rho = \tfrac{1}{2}\dot{\boldsymbol{\rho}}^T\mathbf{M}_{\rho\rho}\dot{\boldsymbol{\rho}}, \quad \mathbf{M}_{\rho\rho} \triangleq \mathbf{J}_\theta^{-T}\mathbf{M}_{\theta\theta}\mathbf{J}_\theta^{-1}$$
$$T_e = \tfrac{1}{2}\dot{\mathbf{q}}_e^T\hat{\mathbf{M}}_{ee}\dot{\mathbf{q}}_e, \quad \hat{\mathbf{M}}_{ee} \triangleq \mathbf{M}_{ee} - \mathbf{M}_{\theta e}^T\mathbf{M}_{\theta\theta}^{-1}\mathbf{M}_{\theta e}.$$

Since the potential energy is $V_e = \frac{1}{2}\mathbf{q}_e^T\mathbf{K}_{ee}\mathbf{q}_e$, and the virtual work is $\delta W_e = \boldsymbol{\tau}^T\delta\boldsymbol{\theta} = \mathbf{u}^T(\delta\boldsymbol{\rho} - \mathbf{J}_e\delta\mathbf{q}_e)$, Lagrange's equations yield

$$\begin{aligned} \mathbf{M}_{\rho\rho}\ddot{\boldsymbol{\rho}} &= \mathbf{u} + \mathbf{f}_{non,\rho}, \\ \mathbf{f}_{non,\rho} &= -\dot{\mathbf{M}}_{\rho\rho}\dot{\boldsymbol{\rho}} + \tfrac{1}{2}\partial(\dot{\boldsymbol{\rho}}^T\mathbf{M}_{\rho\rho}\dot{\boldsymbol{\rho}} \\ &\quad + \dot{\mathbf{q}}_e^T\hat{\mathbf{M}}_{ee}\dot{\mathbf{q}}_e)/\partial\boldsymbol{\rho} \qquad (36) \\ \hat{\mathbf{M}}_{ee}\ddot{\mathbf{q}}_e + \mathbf{K}_{ee}\mathbf{q}_e &= -\mathbf{J}_e^T\mathbf{u} + \mathbf{f}_{non,e}, \\ \mathbf{f}_{non,e} &= -\dot{\hat{\mathbf{M}}}_{ee}\dot{\mathbf{q}}_e + \tfrac{1}{2}\partial(\dot{\boldsymbol{\rho}}^T\mathbf{M}_{\rho\rho}\dot{\boldsymbol{\rho}} \\ &\quad + \dot{\mathbf{q}}_e^T\hat{\mathbf{M}}_{ee}\dot{\mathbf{q}}_e)/\partial\mathbf{q}_e, \qquad (37) \end{aligned}$$

which are coupled by virtue of the configuration dependence of $\mathbf{M}_{\rho\rho}$, $\widehat{\mathbf{M}}_{ee}$, $\mathbf{J}_\theta$, and $\mathbf{J}_e$.

Although the mass matrices $\mathbf{M}_{\rho\rho}$ and $\widehat{\mathbf{M}}_{ee}$ depend on θ and $\mathbf{q}_e$, a suitable approximation is to neglect the elastic coordinate dependence and take $\theta = \mathcal{F}_r^{-1}(\rho)$, where $\mathcal{F}_r(\cdot)$ is the rigid forward kinematics map. If one further neglects the $\mathcal{O}(\|\dot{\mathbf{q}}_e\|^2)$ term in (36), it becomes equivalent to the rigid-body task-space motion equations relating $\mathbf{u}$ to $\dot{\rho}$. On this basis, the rigid inverse dynamics strategy corresponding to a prescribed trajectory ρ_d should produce good endpoint tracking that is consistent with the linear relations in (10)–(12) when $\mu = 1$. The separation of endpoint and elastic dynamics is reminiscent of the singular perturbation approach of Siciliano and Book (1988). In their work, the elastic equations played the role of "fast dynamics" and were similar to (37). However, the analogue of (36) was the joint-space dynamics of the equivalent rigid arm. The assumption of large stiffness led to approximate decoupling, whereas here the decoupling is made possible by relative mass properties independent of the stiffness.

Definining the Hamiltonian $H = T_\rho + T_e + V_e$ and using standard properties of Euler-Lagrange systems (van der Schaft 1996), we have the energy balance $\dot{H} = \mathbf{u}^T(\dot{\rho} - \mathbf{J}_e\dot{\mathbf{q}}_e)$. The approximate form of (36) defined above implies that $\dot{T}_\rho = \mathbf{u}^T\dot{\rho}$, and hence $\dot{T}_e + \dot{V}_e = -\mathbf{u}^T\mathbf{J}_e\dot{\mathbf{q}}_e$. Since $\dot{\rho}_\mu = \dot{\rho} - (1-\mu)\mathbf{J}_e\dot{\mathbf{q}}_e$, we have $\dot{T}_\rho + (1-\mu)(\dot{T}_e + \dot{V}_e) = \dot{\rho}_\mu^T\mathbf{u}$ or, upon integration,

$$\int_0^T \dot{\rho}_\mu^T\mathbf{u}\,dt = \left[T_\rho + (1-\mu)(T_e + V_e)\right]_{t=0}^{t=T}, \qquad (38)$$

which yields passivity of the mapping from $\mathbf{u}$ to $\dot{\rho}_\mu$ when $\mu \leq 1$. For $\mu = 1$, we have passivity but lose observability of the elastic coordinates.

Given the passivity result for $\mu < 1$, many controllers can be constructed that yield setpoint regulation for the end-effector coordinates. In particular, a PD law of the form $\boldsymbol{\tau} = -\mathbf{J}_\theta^T[\mathbf{K}_d\dot{\rho}_\mu + \mathbf{K}_p(\rho_\mu - \rho_d)]$ with $\mathbf{K}_p = \mathbf{K}_p^T > \mathbf{O}$ and $\mathbf{K}_d = \mathbf{K}_d^T > \mathbf{O}$ can be expected to yield $\rho(t) \to \rho_d$ and $\mathbf{q}_e(t) \to \mathbf{0}$ as $t \to \infty$. However, to guarantee this result in the absence of controllability/observability assumptions for $\mathbf{q}_e$, a small damping term of the form $\mathbf{D}_{ee}\dot{\mathbf{q}}_e$ is required on the left-hand side of (37). The Lyapunov function $\mathcal{V} = T_\rho + (1-\mu)(T_e + V_e) + \frac{1}{2}(\rho_\mu - \rho_d)^T\mathbf{K}_p(\rho_\mu - \rho_d)$, in conjunction with the damped form of (38), yields $\dot{\mathcal{V}} = -\dot{\rho}_\mu^T\mathbf{K}_d\dot{\rho}_\mu - \dot{\mathbf{q}}_e^T\mathbf{D}_{ee}\dot{\mathbf{q}}_e$. Hence, as $t \to \infty$, $\dot{\mathbf{q}}_e(t) \to \mathbf{0}$, $\dot{\rho}_\mu(t) \to \mathbf{0}$, and $\dot{\rho}(t) = \dot{\rho}_\mu + (1-\mu)\mathbf{J}_e\dot{\mathbf{q}}_e \to \mathbf{0}$. LaSalle's theorem with (36) and (37) gives the desired result. The robustness of this stabilization result hinges only on the property in Lemma 1 that has been shown to hold asymptotically for large tip/link mass ratio. Tracking of a time-varying trajectory $\rho_d(t)$ can be accomplished by suitably modifying a feedforward based on (36) and (37) to preserve passivity in the error dynamics (Damaren 1996b).

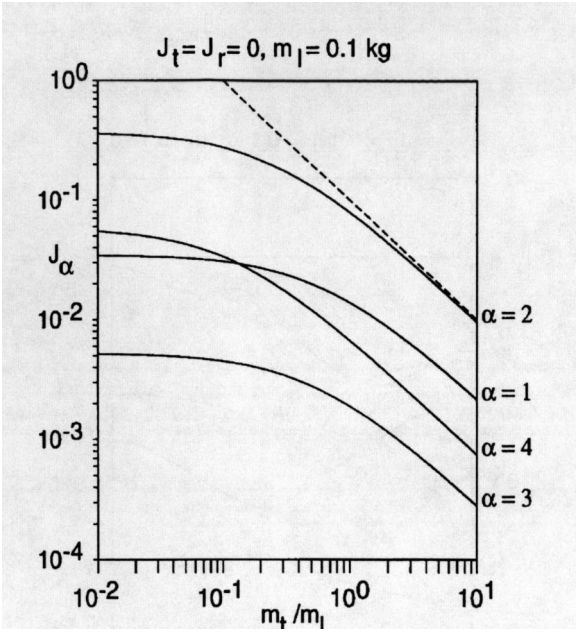

Fig. 2. J_α versus m_t/m_ℓ.

5. Numerical Example

Consider the flexible manipulator of Figure 1 with the following link properties: $\ell_n = \ell = 0.5$ m, $m_{\ell n} = m_\ell = 0.1$ kg, and $(EI)_n = 1$ N·m^2, $n = 1, 2$. We set $J_{tn} = J_t$, $J_{rn} = J_r$, $m_{tn} = m_t$ and initially take $J_t = J_r = 0$ with $\bar{\theta}_2 = \pi/2$. For spatial discretization, the exact cantilevered-free mode shapes of a uniform beam will be used with two per link. The global mass and stiffness matrices can then be formed and used to solve the eigenproblem in (5). With $\mathbf{q}_\alpha$ in hand, J_α in (33) can be formed using the Jacobian matrices in (19).

In Figure 2, the values of J_α for the four unconstrained vibration modes are shown as a function of the mass ratio m_t/m_ℓ. The asymptotic behavior is in agreement with Theorem 1, and for $m_t/m_\ell \geq 10$, we have $J_\alpha < 0.01$. In Figure 3, the configuration dependence of J_α on $\bar{\theta}_2$ is shown for the fixed ratio $m_t/m_\ell = 10$. For all configurations, $J_\alpha < 0.03$.

The effect of tip inertia is portrayed in Figure 4 using the same parameter datum. Note that critical values of J_t force $J_\alpha = 0$, and asymptotically, J_3 and J_4 remain small. Figure 5 shows the variation with rotor inertia that asymptotically destroys the momentum balance required to keep J_α small; however, as predicted, the first-order effect is zero. The vibration modes are shown in Figure 6, where the number of cantilevered shape functions has been increased to 10 per link to improve the accuracy. The most obvious feature is confinement of vibrations to a single link. Convergence to the expected pinned-pinned behavior in each link is in evidence, and the numerical frequencies agree quite well with the exact results for a uniform pinned-pinned beam: $\omega_{1,2} = 14.05$ Hz and $\omega_{3,4} = 56.20$ Hz. Note that in Figure 6, we have illus-

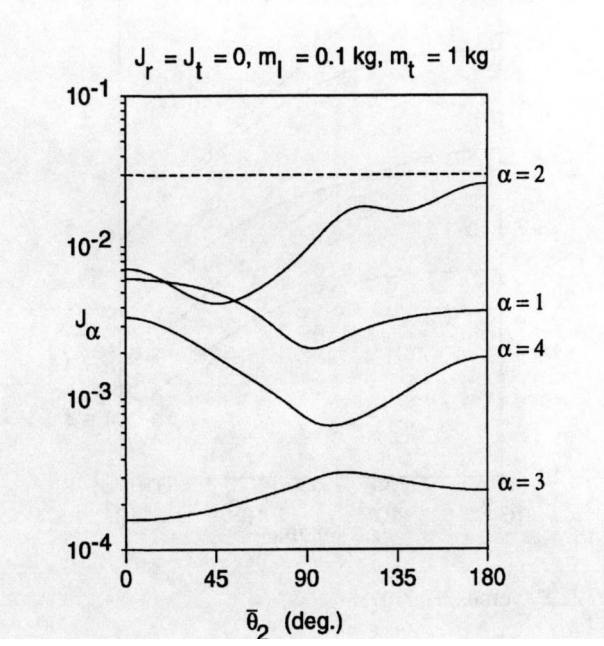

Fig. 3. J_α versus $\bar{\theta}_2$.

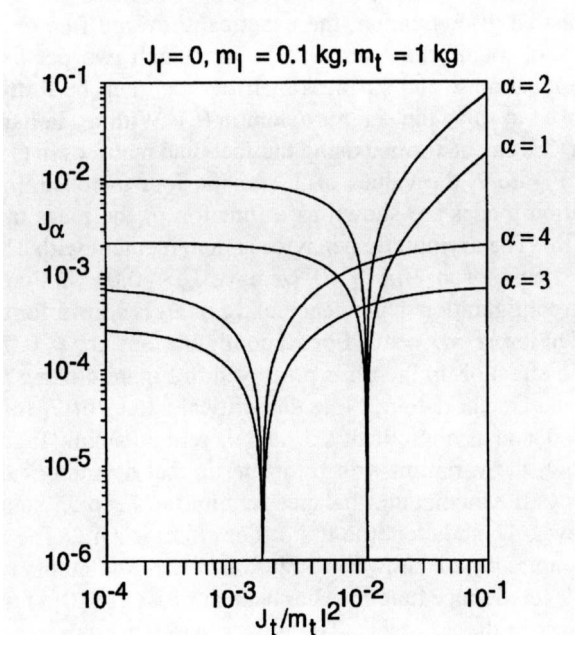

Fig. 4. J_α versus $J_t/m_t\ell^2$.

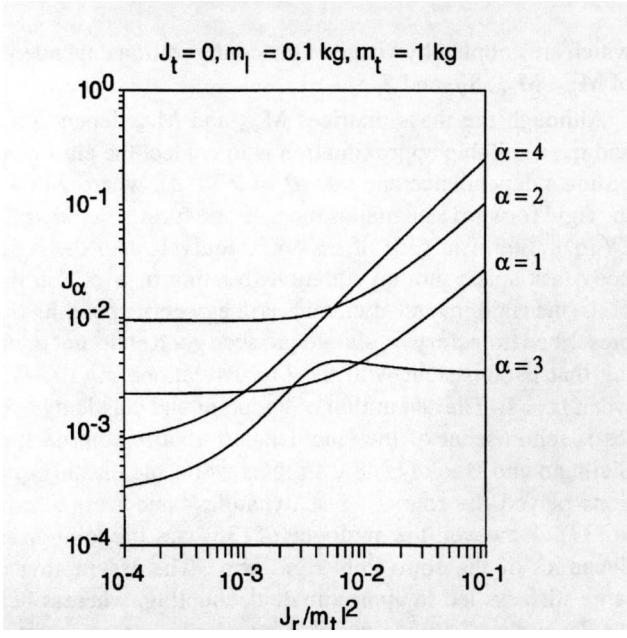

Fig. 5. J_α versus $J_r/m_t\ell^2$.

trated small joint and link motions relative to the L-shaped setpoint.

When 10 modes per link were used to generate Figures 2–5 for $\alpha = 1 \cdots 10$, all reported trends were preserved. The results for $\alpha = 1, 2$ were identical, reflecting their converged nature using two modes per link. The rolloff for $\alpha = 4 \cdots 10$ in Figure 2 was similar, and these curves all fell beneath that of $\alpha = 3$; roughly speaking, J_α falls off with α. For Figure 3, five of the modes ($\alpha = 1, 4, 5, 8, 9$) exhibit a minimum for J_α in the vicinity of $\bar{\theta}_2 = 90°$. The sharp pairwise minimum exhibited by Figure 4 was maintained for all 10 modes with adjacent modes pairing. The location of the minimum (value of $J_t/(m_t\ell^2)$) monotonically decreased with α. The analogue of Figure 5 showed that six modes asymptotically obey $J_\alpha \propto J_r/(m_t\ell^2)$, whereas those corresponding to $\alpha = 3, 5, 7$, and 9 asymptoted to constant values of $J_\alpha < 0.004$. Hence, the presence of large rotor inertias does not destroy the key property in all modes.

Although experimental results are not presented here, we draw the reader's attention to the interesting work of Oakley and Cannon (1989b). They used multiple-exposure photography to capture the first four mode shapes of a two-link flexible arm with joint/tip-dominated mass distribution. There is general agreement between our results and their photographs. In particular, their photographs are qualitatively similar to Figure 6. Furthermore, modes 1, 3, and 4 in their figures exhibit little discernible motion at the manipulator endpoint. Mode 2 showed the greatest motion, and a value of $J_\alpha \doteq 0.17$ was crudely determined from their photographs. This is in general agreement with Figure 2. The numerical properties of the arm provided by Oakley and

$\alpha = 1,\ \omega_1 = 14.06\,\text{Hz}$

$\alpha = 3,\ \omega_3 = 56.19\,\text{Hz}$

$\alpha = 2,\ \omega_2 = 14.06\,\text{Hz}$

$\alpha = 4,\ \omega_4 = 56.20\,\text{Hz}$

Fig. 6. Unconstrained mode shapes ($m_t/m_\ell = 10, J_t = J_r = 0, \bar{\theta}_2 = \pi/2$).

Cannon (1989a) are $\ell_n = 0.52$ m, $(EI)_n = 0.77\ \text{N}\cdot\text{m}^2$, $n = 1,2$, $m_{\ell 1} = 0.38\,\text{kg}$, $m_{\ell 2} = 0.37$ kg, $J_{r1} = 0.0039\ \text{kg}\cdot\text{m}^2$, $m_{t1} = 0.56\,\text{kg}$, $J_{t1} = 0.0013\ \text{kg}\cdot\text{m}^2$, $m_{r2} = 1.34$ kg, $J_{r2} = 0.0029\,\text{kg}\cdot\text{m}^2$, $m_{t2} = 0.37$ kg, and $J_{t2} = 0.00077\ \text{kg}\cdot\text{m}^2$. There were also mechanical offsets at the inboard end of link 2 and the outboard ends of links 1 and 2. When a complete model incorporating these latter effects was used with 10 cantilevered modes per link, we were able to accurately predict their frequencies ($\omega_1 = 3.4$ Hz, $\omega_2 = 4.0$ Hz, $\omega_3 = 8.9$ Hz, and $\omega_4 = 12.2$ Hz). The corresponding values for the J_α were $\mathsf{J}_1 = 0.010$, $\mathsf{J}_2 = 0.100$, $\mathsf{J}_3 = 0.011$, and $\mathsf{J}_4 = 0.016$, which agrees with the above observations.

We now consider control of an identical link configuration with the properties given in Table 1. The goal is to move the end-effector from a fully extended configuration ($\theta_1 = \theta_2 = 0$) to an L-shaped configuration with $\theta_1 = \theta_2 = \theta_d = \pi/2$ in $T = 5$ s. For this purpose, we use the end-effector trajectory obtained via the rigid kinematics corresponding to

$$\theta_n(t) = \theta_d \left(\frac{t}{T} - \frac{1}{2\pi} \sin \frac{2\pi t}{T} \right), \quad n = 1,2.$$

The response of the arm to the corresponding rigid inverse dynamics torques $\boldsymbol{\tau}_{inv}$ is portrayed in Figure 7. The simulation results presented here have been generated using a recursive implementation of the fully nonlinear motion equations. See the I(E) model discussed in detail by Damaren and Sharf (1995).

As might be expected, the joint-space tracking is fairly poor and exhibits significant vibration. However, very little vibration is seen at the end-effector, and good tracking is obtained. A small steady-state rate discrepancy is present that leads to the growth of the x- and y-tracking errors.

In the interests of improved tracking, stability, and robustness, the feedforward can be augmented with the feedback proposed in Section 5. The applied torque is given by

$$\boldsymbol{\tau}(t) = \boldsymbol{\tau}_{inv}(t) - \mathbf{J}_\theta(\boldsymbol{\theta}, \mathbf{0})^T [\mathbf{K}_d(\dot{\boldsymbol{\rho}}_\mu - \dot{\boldsymbol{\rho}}_d) + \mathbf{K}_p(\boldsymbol{\rho}_\mu - \boldsymbol{\rho}_d)]. \tag{39}$$

The μ-tip rate can be written as

$$\dot{\boldsymbol{\rho}}_\mu = \mathbf{J}_\theta \dot{\boldsymbol{\theta}} + \mu \mathbf{J}_e \dot{\mathbf{q}}_e \doteq \mu \dot{\boldsymbol{\rho}} + (1-\mu)\mathbf{J}_\theta(\boldsymbol{\theta}, \mathbf{0})\dot{\boldsymbol{\theta}},$$

and hence $\boldsymbol{\rho}_\mu \doteq \mu\boldsymbol{\rho} + (1-\mu)\boldsymbol{\mathcal{F}}(\boldsymbol{\theta}, \mathbf{0})$. Note that the rigid Jacobian is evaluated using only joint measurements so that $\boldsymbol{\rho}_\mu$ and $\dot{\boldsymbol{\rho}}_\mu$ can be formed without measurements of the elastic coordinates. Although a simple PD law is used here, the derivative gain can be replaced with a dynamic, strictly positive real controller or even a gain-scheduled version, which preserves stability (Damaren 1996c).

The value of μ is set at 0.96, which is small enough to affect the observability of the vibration modes but near enough to unity so that the desired value of $\boldsymbol{\rho}_\mu$ can be approximated by $\boldsymbol{\rho}_d$ in the feedback part of the controller. The feedback gains are taken to be $\mathbf{K}_p = (4\ \text{rad/s})^2 \mathbf{M}_{\theta\theta}(\boldsymbol{\theta}_d, \mathbf{0})$ and $\mathbf{K}_d = (8\ \text{rad/s})\mathbf{M}_{\theta\theta}(\boldsymbol{\theta}_d, \mathbf{0})$. The resulting tracking errors and joint rate behavior are given in Figure 8. Steady-state tracking is much improved, with a minor increase in transient errors, but significant vibration suppression is observed at the joint level. Improved tracking can be obtained if $\boldsymbol{\rho}_d$ is replaced by $\boldsymbol{\rho}_{\mu d}$, which requires solving the flexible inverse kinematics problem to obtain the corresponding $\mathbf{q}_{ed}$ and $\boldsymbol{\theta}_d$.

Table 1. Flexible Manipulator Properties

$\ell = 0.5$ m, $m_\ell = 0.1$ kg, $EI = 1\ \text{N}\cdot\text{m}^2$
$m_t = 1$ kg , $J_t = J_r = 0.001\ \text{kg}\cdot\text{m}^2$

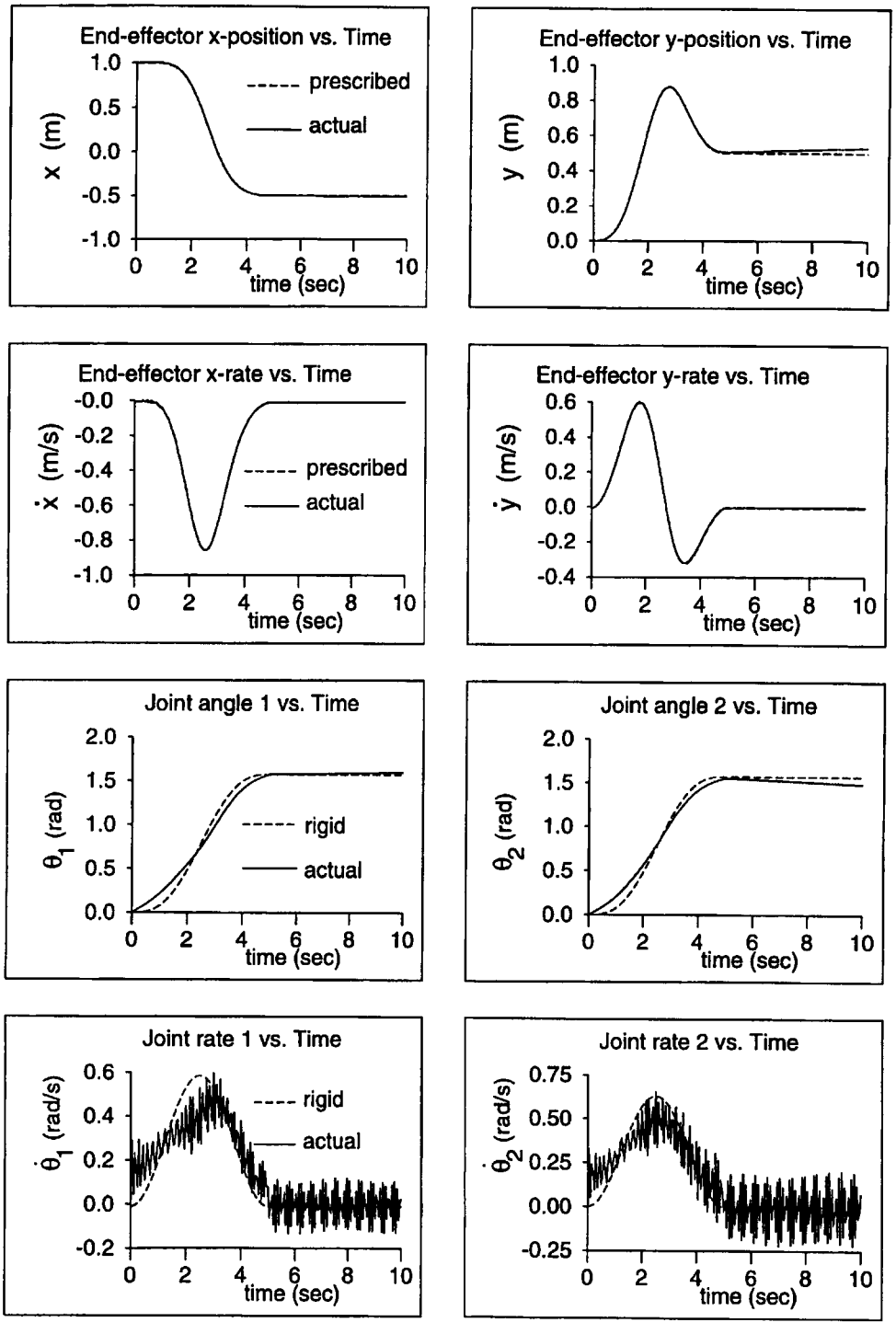

Fig. 7. Response to rigid inverse dynamics.

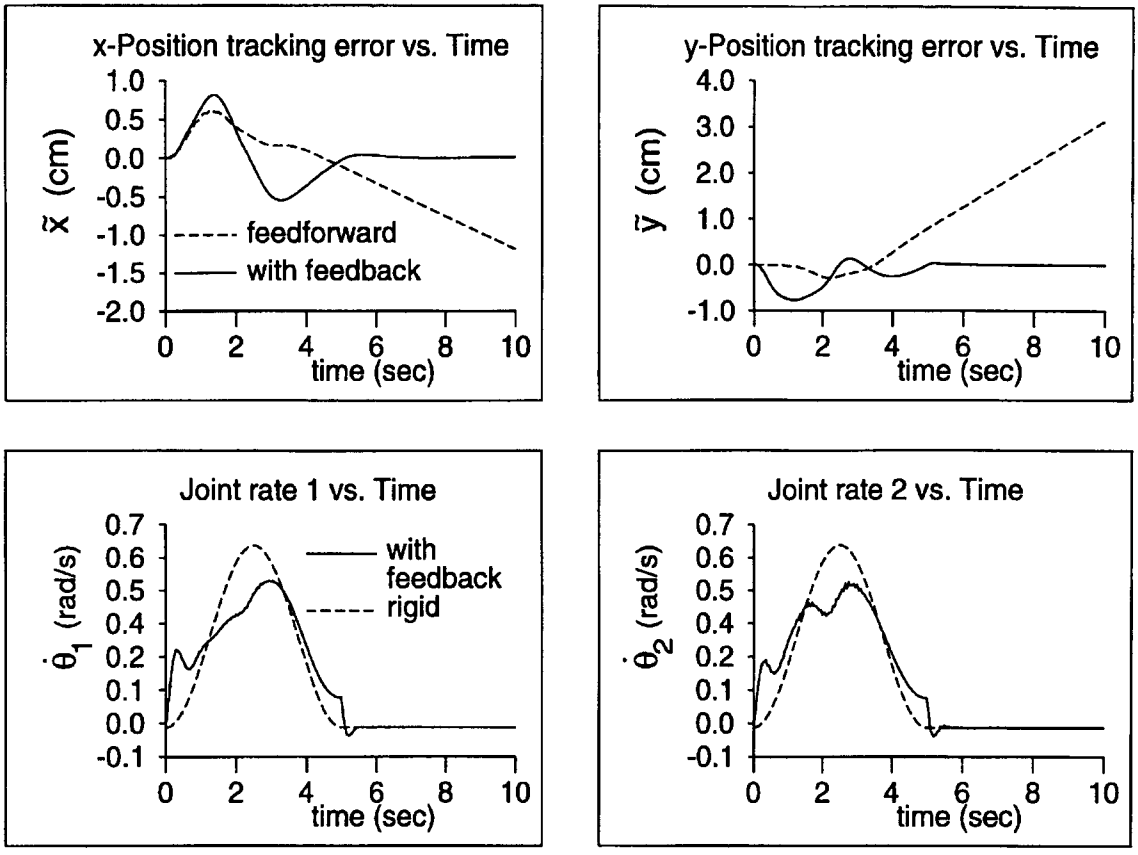

Fig. 8. Responses for rigid feedforward/μ-tip PD feedback.

6. Conclusions

A necessary and sufficient condition for the vibration modes of a serial flexible manipulator to exhibit a node at the end-effector has been presented. An explicit treatment of the two-link case has shown that this condition is nearly achieved for large tip/link mass ratio, and the effect of the other parameters was determined. The ensuing simplified behavior of the torque to endpoint dynamics was demonstrated using nonlinear arguments and illustrated with a numerical example. In particular, a rigid inverse dynamics strategy was shown to invert this mapping quite well. Hence, the well-known nonminimum phase behavior of the mapping is largely mitigated in this asymptotic case.

The results also permitted the synthesis of an output containing contributions from the end-effector coordinates and the elastic motion of the robot. This output possesses the passivity property that permits simultaneous endpoint tracking and vibration suppression to be handled in a simple robust manner. Although endpoint measurements are required, the proposed output dispenses with the need to measure the elastic coordinates and their rates.

The raison d'être of structurally flexible robots lies in increased payload/robot mass capability and increased speed of operation. This leads to minimization of link mass coupled with inherent limitations on possible mass reduction of the electromagnetic actuators. The importance of our results lies in the closeness with which they mirror this situation.

Acknowledgment

The author gratefully acknowledges financial support provided by the University of Canterbury in the form of Research Grant 2201999.

References

Anderson, B.D.O., and Vongpanitlerd, S. 1973. *Network Analysis and Synthesis*. Englewood Cliffs, NJ: Prentice Hall.

Barbieri, E. 1993. Single-input/single-output transfer functions for a flexible slewing link. *J. Robotic Sys.* 10(7):913–929.

Bayo, E., Papadopoulos, P., Stubbe, J., and Serna, M. 1989. Inverse dynamics and kinematics of multi-link elastic robots: An iterative frequency domain approach. *Int. J. Robotics Research* 8(6):49–62.

Book, W. J. 1993a. Controlled motion in an elastic world. *ASME J. Dyn. Sys. Meas. Control* 115:252–261.

Book, W. J. 1993b. Structural flexibility of motion systems in the space environment. *IEEE Trans. Robotics and Automation* 9(5):524–530.

Book, W. J., Maizza-Neto, O., and Whitney, D. E. 1975. Feedback control of two beam, two joint systems with distributed flexiblity. *ASME J. Dyn. Sys. Meas. Control* 97G(4):424–431.

Canudas de Wit, C., Siciliano, B., and Bastin, G., eds. 1996. *Theory of Robot Control*. London: Springer-Verlag.

Damaren, C. J. 1995. Passivity analysis for flexible multilink space manipulators. *AIAA J. Guidance, Control, and Dynamics* 18(2):272–279.

Damaren, C. J. 1996a. Adaptive control of flexible manipulators carrying large uncertain payloads. *J. Robotic Sys.* 13(4):219–228.

Damaren, C. J. 1996b. Approximate inverse dynamics and passive feedback for flexible manipulators with large payloads. *IEEE Trans. Robotics and Automation* 12(1):131–138.

Damaren, C. J. 1996c. Gain scheduled SPR controllers for nonlinear flexible systems. *ASME J. Dyn. Sys. Meas. Control* 118(4):698–703.

Damaren, C. J., and Sharf, I. 1995. Simulation of flexible-link manipulators with inertial and geometric nonlinearities. *ASME J. Dyn. Sys. Meas. Control* 117(1):74–87.

Damaren, C., Stanway, J., and Sharf, I. 1995 (May 1989, Victoria, Canada). Modal analysis for an experimental flexible manipulator. *Proc. 15th Canadian Congress on Applied Mechanics*. Victoria, British Columbia: University of Victoria, vol. 2, pp. 806–807.

De Luca, A., Lucibello, P., and Ulivi, G. 1989. Inversion techniques for trajectory control of flexible robot arms. *J. Robotic Sys.* 6(4):325–344.

De Luca, A., and Siciliano, B. 1993. Inversion-based nonlinear control of robot arms with flexible links. *AIAA J. Guidance, Control, and Dynamics* 16(6):1169–1176.

Desoer, C. A., and Vidyasagar, M. 1975. *Feedback Systems: Input-Output Properties*. New York: Academic Press.

Gevarter, W. B. 1970. Basic relations for control of flexible vehicles. *AIAA J.* 8(4):666–672.

Newcomb, R. W. 1966. *Linear Multiport Synthesis*. New York: McGraw-Hill.

Oakley, C. M., and Cannon, R. H. Jr. 1989a (San Francisco, December). Equations of motion for an experimental two-link flexible manipulator. *Proc. ASME Winter Annual Meeting*. New York: ASME, pp. 267–278.

Oakley, C. M., and Cannon, R. H. Jr. 1989b (Montreal, June). Theory and experiments in selecting mode shapes for two-link flexible manipulators. *Proc. Experimental Robotics I—First International Symposium*, pp. 1–19.

Paden, B., Chen, D., Ledesma, R., and Bayo, E. 1993. Exponentially stable tracking control for multijoint flexible-link manipulators. *ASME J. Dyn. Sys. Meas. Control* 115(1):53–59.

Park, J.-H., and Asada, H. 1994. Dynamic analysis of non-collocated flexible arms and design of torque transmission mechanism. *ASME J. Dyn. Sys. Meas. Control* 116:201–207.

Pota, H. R., and Vidyasagar, M. 1991 (April, Sacramento, CA). Passivity of flexible beam transfer functions with modified outputs. *Proc. IEEE Int. Conf. Robotics and Automation*. New York: IEEE, vol. 2, pp. 2826–2831.

Siciliano, B., and Book, W. J. 1988. A singular perturbation approach to control of lightweight flexible manipulators. *Int. J. Robotics Research* 7(4):79–90.

van der Schaft, A. 1996. *L_2-Gain and Passivity Techniques in Nonlinear Control*. London: Springer-Verlag.

Wang, D., and Vidyasagar, M. 1990 (April, Cincinnati, OH). Passive control of a single flexible link. *Proc. IEEE Int. Conf. Robotics and Automation*. New York: IEEE, vol. 2, pp. 1432–1437.

Wang, D., and Vidyasagar, M. 1992. Transfer functions for a single flexible link. *Int. J. Robotics Research* 10(5):540–549.

Yim, W. 1993 (May, Altanta, GA). End-point trajectory control, stabilization, and zero dynamics of a three-link flexible manipulator. *Proc. IEEE Int. Conf. Robotics and Automation*. New York: IEEE, vol. 2, pp. 468–473.